KSOE

Journal of Ocean Engineering and Technology 39(1), 73-81, February, 2025 eISSN 2287-6715
https://doi.org/10.26748/KSOE.2024.092

Original Research Article

Numerical Simulation of Unsteady Flow Past a Rotating Wells Turbine with Modified Blades

Eru Kurihara[1], Hiroki Yasui[2], Yuito Isayama[2] and Hiromitsu Hamakawa[3]

[1]*Associate Professor, Faculty of Science and Technology, Oita University, Oita, Japan*
[2]*Graduate Student, Graduate School of Engineering, Oita University, Oita, Japan*
[3]*Proffesor, Faculty of Science and Technology, Oita University, Oita, Japan*

KEYWORDS: Wells turbine, Large eddy simulation (LES), serration, airfoil cascade, wave power

ABSTRACT: *Wells turbines used in wave power generation have the advantage of being usable in reciprocating flow, but they also face many unsolved problems, such as self-starting performance, low efficiency, and noise. The purpose of this study is to assess the effect of serrations added to symmetrical blades used in Wells turbines on stall characteristics and lift-drag ratio. In this study, large eddy simulation was employed as numerical method to clarify the spatio-temporal behavior of the flow field, including flow rate fluctuations. In addition to turbine blade modifications, this study also evaluated the effect of changes in rotor solidity on turbine performance. The results show that the serrated turbine had up to a 30% increase in torque over the normal-blade turbine. Additionally, power fluctuations caused by blade stalling were also suppressed. For a tandem arrangement of blades, the effect of wake flow from the front blades on the rear blades was evaluated. Simulations of a serrated blade cascade and turbine rotors have shown that serration processing can improve the performance of Wells turbines. It was also found that not only the interaction between serrated blades but also the serrations themselves have a significant effect on airfoil performance.*

1. Introduction

Global warming and increasing global energy demand are major issues worldwide. Therefore, wave and wind power generation, which obtain energy from nature, are attracting significant attention (Takao et al., 2019; Takao et al., 2002). Regarding the use of ocean energy, the Wells turbine is a known source of oscillating water column (OWC) power generation (Washio et al., 2000). The simple structure of the turbine is expected to lower the cost of installation and maintenance. However, Wells turbines used for wave and wind power generation involve loud operating noise. Noise from such fluid machinery can cause acoustic pollution of the marine environment. Reducing noise and improving the turbine performance are important issues in promoting the use of the turbine (Teruna et al., 2021). Suzuki and Arakawa (2008b) experimentally investigated the effect of Wells turbine blade geometry on the surrounding flow. They measured the torque coefficient, pressure drop, efficiency, and flow field behind the rotor blades using the oil film method. Suzuki and Arakawa (2001) also numerically analyzed the flow around the Wells turbine. The velocity field around the blade was visualized by steady state calculation using the SIMPLE algorithm with a cyclic boundary condition. The results obtained from the numerical solution and oil film method were compared in that study.

Various studies have been conducted on the performance design of Wells turbines. Soltanmohamadi and Lakzian (2016) proposed optimization of the blade chord length of a Wells turbine using numerical simulation. Cui and Hyun (2016) numerically analyzed the effect of guide vanes on the turbine efficiency. The results agreed well with corresponding experimental data obtained by Takao et al. (2001). Kumar et al. (2018) compared the reference blade with undulated turbine blades for a Wells turbine using steady Reynolds averaged Navier-Stokes (RANS) simulations. The results showed the difference in flow around the reference and serrated blades. In that study, they introduced undulations to the leading edge of the blades. There have been many fundamental studies of serration processing on airfoils through experiments and numerical simulations (Cao et al. (2020);

Received 6 November 2024, revised 11 December 2024, accepted 7 February 2025
Corresponding author Eru Kurihara: +81-97-554-7779, kurihara@oita-u.ac.jp
This is a paper from the proceedings of 2024 Asian Offshore Wind, Wave, and Tidal Energy Conference held in Busan, Korea (Kurihara et al., 2024).

Hussain et al. (2017); Liu et al. (2015)). Liu et al. (2015) introduced serrations in airfoils and experimentally demonstrated their improvement to the aerodynamic performance. Hussein et al. conducted experiments and RANS calculations for trailing edge serrated airfoils and showed improved lift–drag ratios at high angle of attack. Cao et al. (2020) confirmed the effect of noise reduction in trailing edge serrated airfoils by large eddy simulation (LES) analysis. In their study, LES analysis was performed for a trailing edge serrated airfoil cascade to investigate the effect of the wake on flow around the following airfoil. Regarding the geometric design of turbine rotors, more recently, the performance design of the Wells turbine using computational fluid dynamics (CFD) optimization was performed by Kotb et al. (2023). Their work was carried out by RANS with a 1/8 section turbine model, which did not well-represent the unsteady flow past the turbine and non-periodic behavior of the circumferential direction.

In this study, the effect of leading or trailing edge serrations of a rotating Wells turbine under transient flow conditions was numerically investigated by LES. Numerical simulations for airfoil cascade were also performed to investigate the detailed effect of the serrations on the flow around the blade.

2. Computational Methodology

In this study, an unsteady flow past a rotating Wells turbine was numerically investigated using incompressible LES. In addition, a numerical analysis for a two-dimensional airfoil cascade was performed to evaluate the effect of serration processing on the flow. Details of the analysis method and models are given below.

2.1 Model of Airfoil Cascade

For the analysis of the airfoil cascade, as shown in Figs. 1 (a) and (b), numerical simulation was performed for flow past two symmetrical airfoils arranged in series. The model is an NACA0021 symmetrical airfoil with a chord length and width of 1000 mm each. The forward airfoil has serrations with a pitch of 165 mm and depth of 55 mm. The gap between the airfoils is 1.0 m. The computational grid for the airfoil cascade is shown in Fig. 1(c). The dimensions of the domain are x = 15 m, y = 10 m, and z = 2 m. Wall-adapting local eddy-viscosity (WALE) model is used as the turbulence model, and the logarithmic law is applied to the boundary condition on the airfoil surface to reproduce the separation of the boundary layer from the surface. The dimensionless thickness y^+ of the first layer is approximately 5, and the total number of meshes is 29.5 million. Therefore, in the present study, it is considered that the flow near the boundary can be reproduced by the WALE model.

2.2 Turbine Models

The turbine models used in this study are based on the corresponding experimental setup (Hamakawa et al., 2015). Numerical models of the normal turbine (reference turbine) and serrated turbine (trailing edge serration) are shown in Figs. 2 (a) and (b), respectively. Every rotor has 8 turbine blades with the NACA0021. The turbine dimensions are l = 100 mm for the chord length and h = 125 mm for

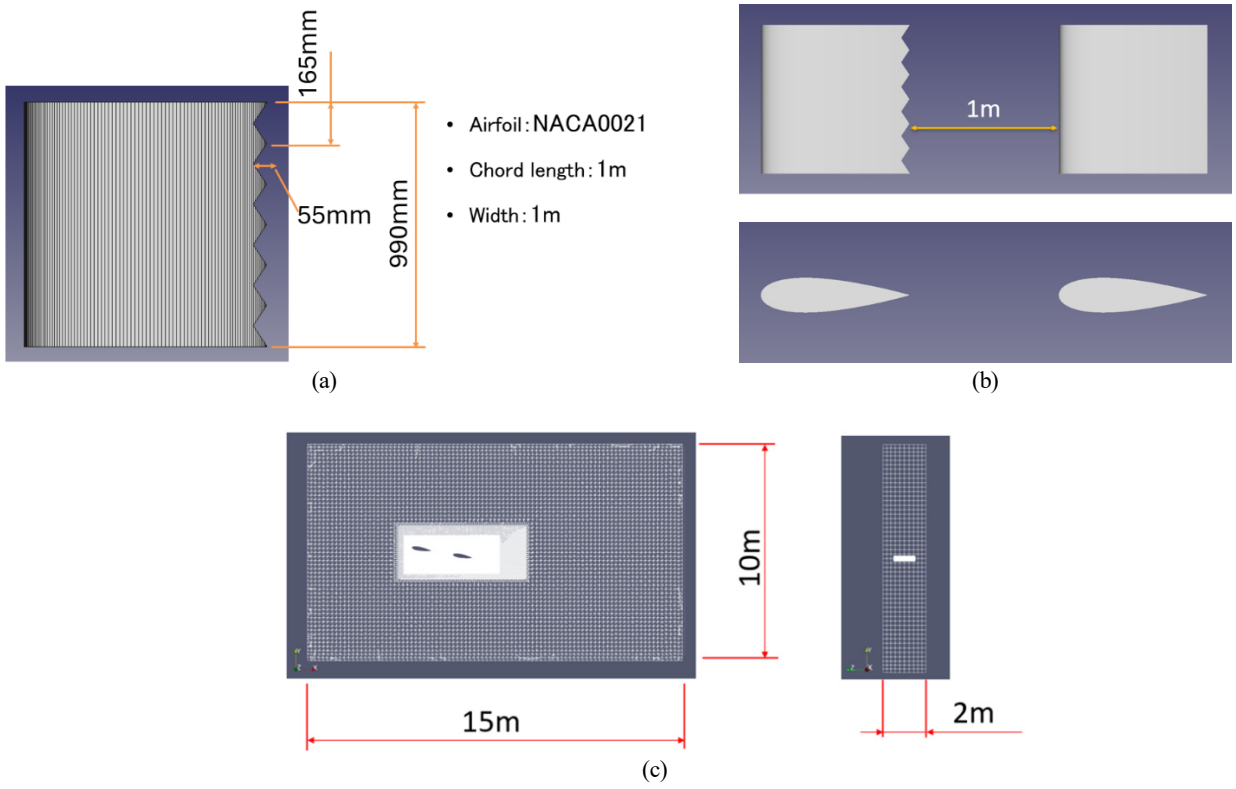

Fig. 1 Schematic of airfoil cascade (a), (b) and calculation domain (c)

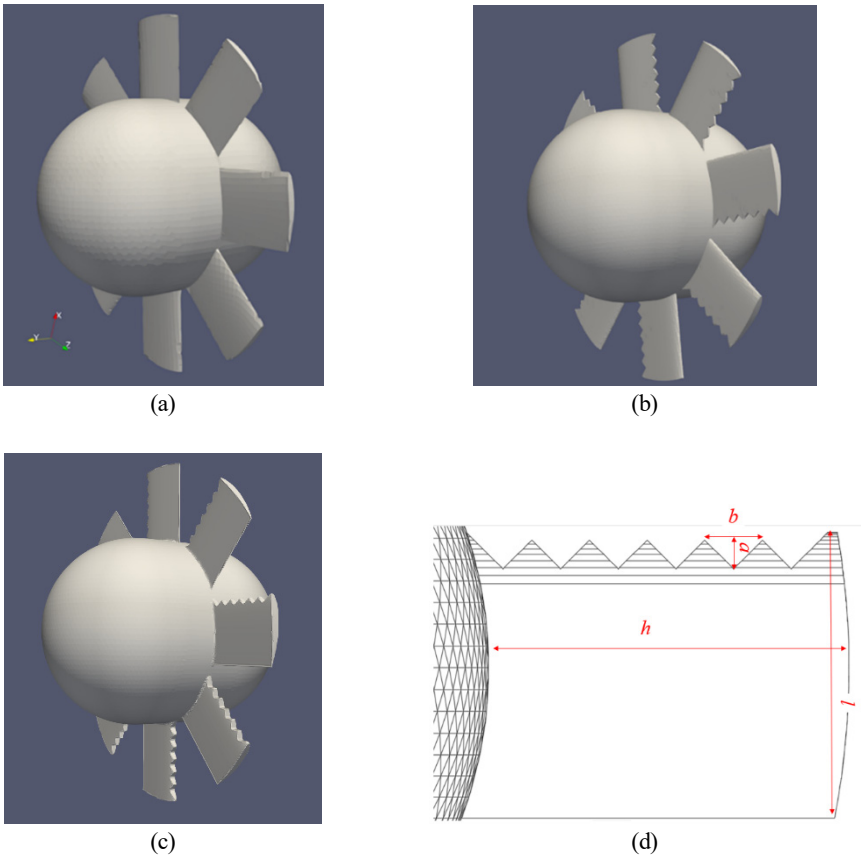

Fig. 2 Schematic view of reference turbine (a), turbine with trailing edge serrations (b), turbine with leading edge serrations (c), and serrated turbine blade (d)

the blade span. The hub diameter is 300 mm, and the casing diameter is 578 mm. For the serrated turbine blade shown in Fig. 2(c), the serration depth and width are a = 12.0 mm and b = 6 mm, respectively. In these models, rotor solidity is 0.68 for the reference turbine and 0.64 for the serrated turbine.

The computational grid for the normal turbine is shown in Figs. 3 (a) and (b). The axial length of the domain is 1600 mm, and the diameter, which corresponds to casing inner diameter, is 578 mm. The total mesh number of is approximately 15 million.

The turbine rotates constantly at 763 rpm (80 rad/s). The inlet velocity increases monotonously with half-cosine ramp from 0 to the maximum velocity (*Umax*) in 0.3 s. In this study, calculations were performed for *Umax* =5.0 and 2.5 m/s. The WALE model (Nicoud and Ducros, 1999) is used for the turbulence model, and the logarithmic law is applied to the solid surface including the turbine rotor. For rotating turbines, two types of calculation method were used in this study: the dynamic mesh method and multiple reference frame (MRF) approach. The MRF approach is an analytical method for non-inertial systems, which applies the rotation effects, such as centrifugal and Coriolis forces, as an additional source term in the momentum equations in the OpenFOAM solvers.

2.3 Dependence on Mesh Resolution

In this study, three different resolutions of the reference turbine model were tested to investigate the dependence of the analysis results on the resolution of the computational grid. The grid numbers of the

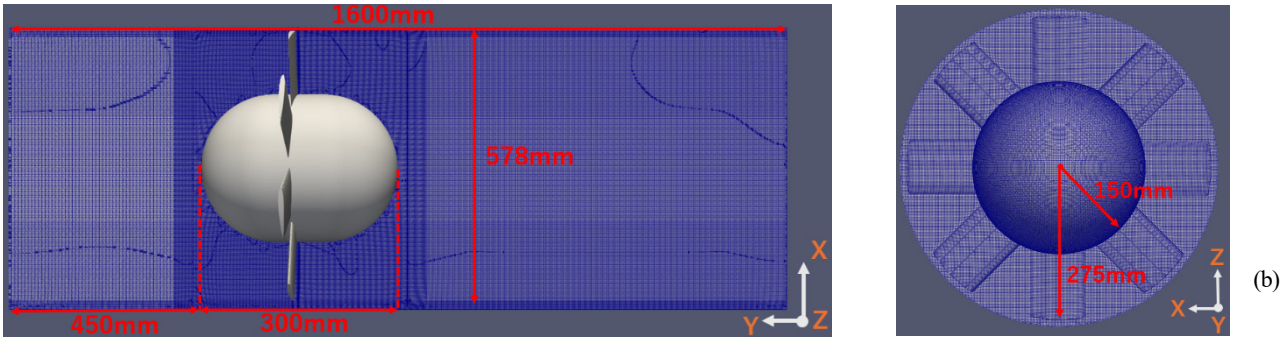

Fig. 3 Computational grid for the normal turbine (side view (a) and front view (b))

Table 1 Averaged values of y^+ on the turbine surface

Grid model	M1	M2	M3
y^+ (at t = 0.2 s)	28.0	16.5	14.5
y^+ (at t = 0.3 s)	27.7	16.8	15.0

three different resolution meshes (M1, M2, and M3) are approximately 10 million for M1, 25 million for M2, and 50 million for M3, respectively. The averaged values of dimensionless thickness y^+ of the computational grid, evaluated by shear velocity at the turbine surface at t = 0.2 and 0.3 s, are shown in Table 1. Because $y^+ < 50$ in all cases, it is confirmed that the approximation of the boundary conditions by the wall function works effectively.

Fig. 4 shows the time evolution of axial torque of the reference turbine calculated using the M1, M2, and M3 grids. Solid lines are the results from the Smagorinsky model, and dashed lines are the results from the WALE model. It can be observed that the results with the M1 grid are significantly different compared to those of other cases. Before a stall occurs (t < 0.2 s), the results for M2 and M3 show good agreement. Then, for t > 0.2 s, there are some differences between the Smagorinsky model results with the M2 and M3 grids. Based on the above results, LES analysis of a rotating turbine model was performed using a grid with a resolution equivalent to that of M2 and the WALE model.

3. Results and Discussion

3.1 Airfoil Cascade

Fig. 5 shows dependence of lift-drag ratio on angle of attack for the cascaded airfoils at Re = 1.0×10^5. Solid and dashed lines indicate results for the front and rear airfoils, respectively. Red lines correspond to the results for airfoil cascade with trailing edge serrations, and the blue lines correspond to the reference airfoil cascade. The results show that the forward serrated wing has a remarkable lift–drag ratio at a = 5°. Figs. 6 (a) and (b) show the velocity distribution in the central section of the airfoil cascade a = 5° for the trailing edge serrated and reference blades, respectively. Dashed lines in the figures correspond to the rotating plane of the turbine blades. Comparing the flow around the forward airfoils in Figs. 6 (a) and (b), a significant flow separation can be observed on the reference wing. Meanwhile, partial detachment can be observed on the serrated blades, but the area is smaller than on the reference blades. Furthermore, in Fig. 6, lift force is lower than that of the forward airfoil because the upper area of the rear wing is in the wake region of the forward airfoil. For $a \geqq 10°$, there is no difference between the serrated and reference airfoils. This can be explained by the fact that, at large angle of attack, the flow is detached at the leading edge of the forward airfoil.

3.2 Wells Turbine

As shown in Fig. 4, the turbine shaft torque does not increase after time t = 0.2 s, regardless of the increase in inflow velocity. This suggests that turbine blade stall occurs after the time in the reference turbine. To determine the reason for this, a comparison of the flow field in the reference and trailing edge serration turbines is performed before and after t = 0.2 s.

Figs. 7 (a) and (b) show pressure distribution on the suction side of the reference turbine for $Umax$ = 0.5 m/s at t = 0.15 s and t = 0.30 s, respectively. As shown in Fig. 4, it can be assumed that the blade stalling does not occur at t = 0.15 s. Fig. 7 (a) shows that the results are in good agreement with the flow pattern and pressure distribution obtained by Suzuki et al. (2008a). In contrast, in Fig. 7 (b), the presence of low-pressure areas and their irregular fluctuations associated with flow separation from the turbine blades are observed.

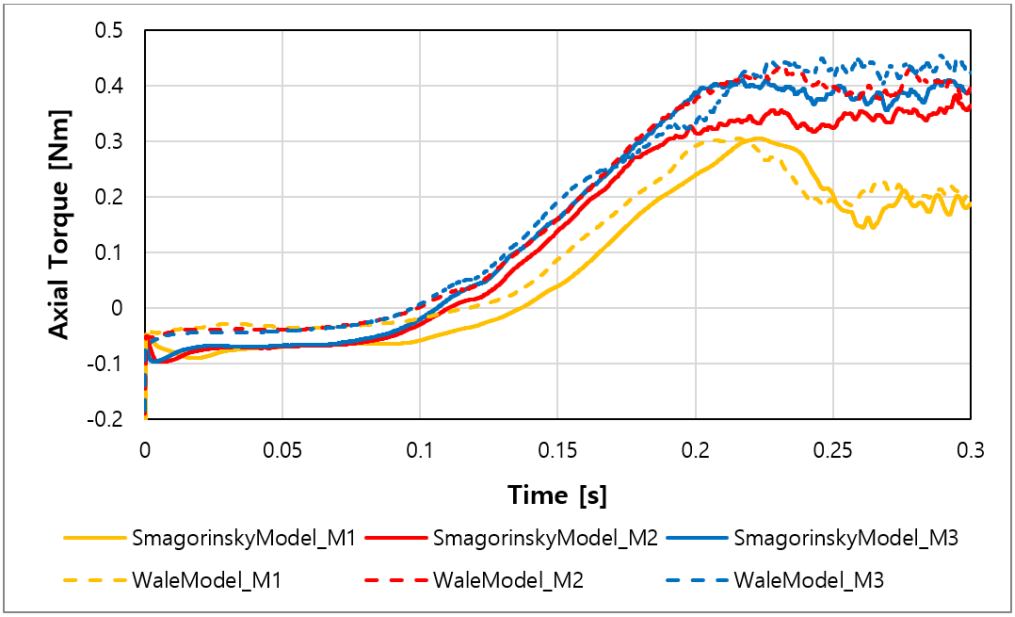

Fig. 4 Dependence of turbine axial torque on grid resolution and turbulence model for the reference turbine

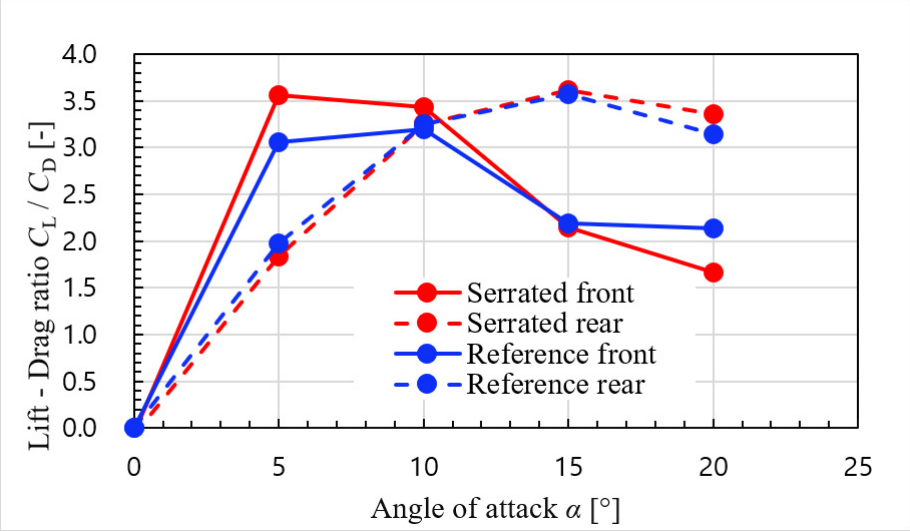

Fig. 5 Dependence of lift–drag ratio on angle of attack for the cascaded airfoils at Re = 1.0×10^5. Solid and dashed lines indicate results for the front and rear airfoils, respectively

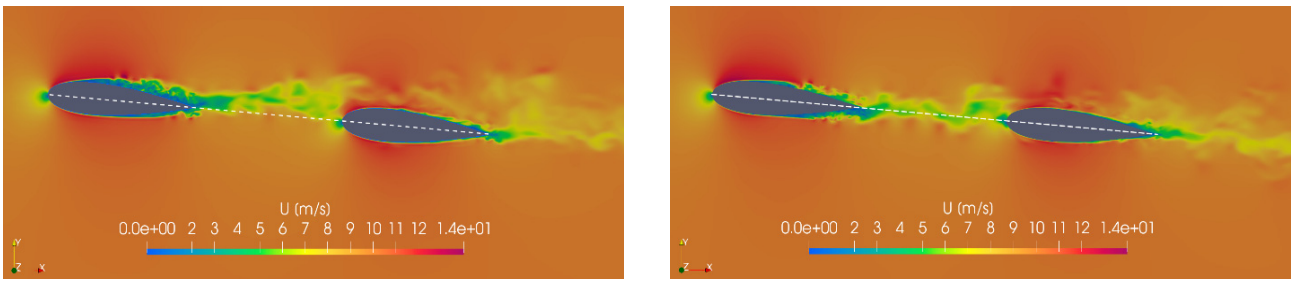

Fig. 6 Velocity distribution of flow past an airfoil cascade in x-y cross-section ((a) reference airfoil and (b) serrated airfoil). Dashed lines correspond to the rotating plane of the turbine blades.

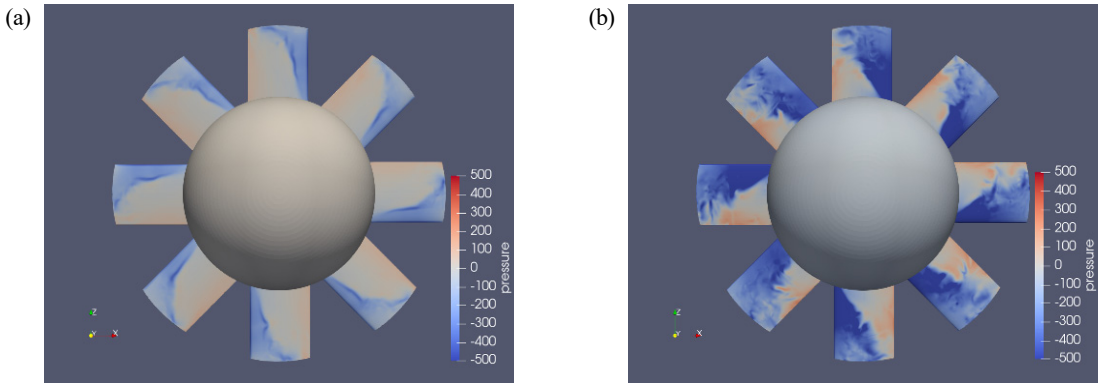

Fig. 7 Pressure distribution on the suction side of the reference normal turbine at t = 0.15 s (a) and t = 0.30 s (b) for $Umax$ = 5 m/s.

This indicates that the turbine is stalled in this condition.

The time responses of the axial torque for the reference turbine (Normal), trailing edge (T. E.) serrated turbine, and leading edge (L. E.) serrated turbine are shown in Fig. 8. The reference turbine has no increase in torque after t = 0.2 s, while the T. E. serrated turbine continues to increase torque as the inlet flow velocity increases. The L. E. serrated turbine, by contrast, always shows significantly lower performance than the reference turbine. The low torque observed even at low angles of attack with low inflow velocities indicates that L. E. serrations promote separation from the leading edge of the blades. Temporal variations in torque are observed after t = 0.2 s in all cases, but the T. E. turbine still shows a torque increase of more than 50% compared to the reference one in this region.

Fig. 9 shows the pressure distribution on the suction side of the turbine with trailing edge serrations at t = 0.30 s. From the figure, the sudden change in pressure associated with flow separation is relatively unclear compared to case of the reference turbine shown in Fig. 7 (b). Therefore, the trailing edge serration blades can obtain relatively

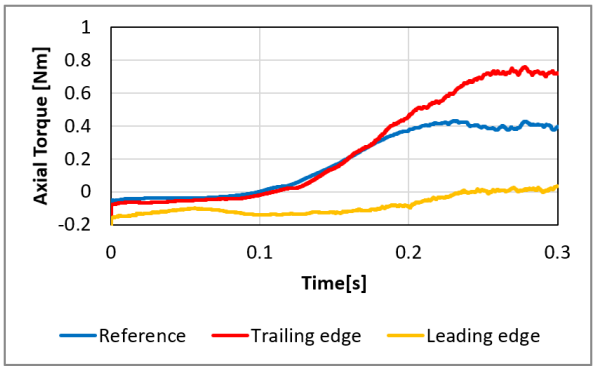

Fig. 8 Time variation of axial torque of reference, trailing edge, and leading edge serrated turbine for *Umax* = 5.0 m/s

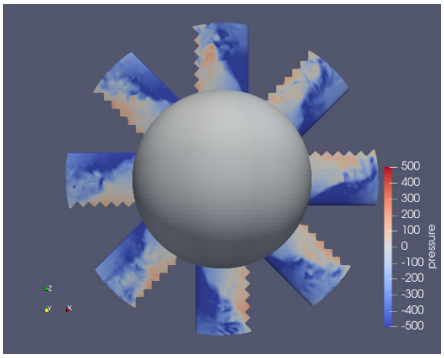

Fig. 9 Pressure distribution on the suction side of the turbine with trailing edge serrations at t = 0.30 s for *Umax* = 0.5 m/s

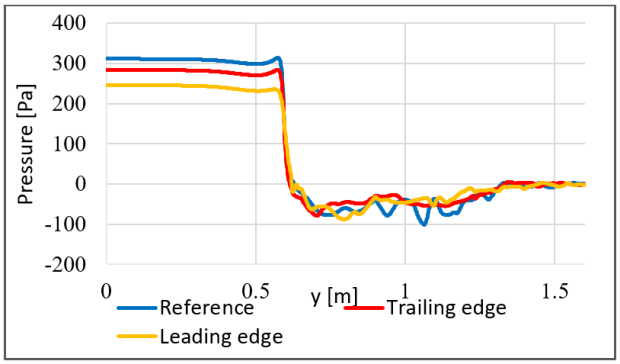

Fig. 10 Pressure distribution in the turbine casing at t = 0.3 s

stable and large torque even in the high angle of attack condition.

Fig. 10 shows pressure distributions in the turbine casing along the x axis at t = 0.3 s. In this calculation, p = 0 is set as the boundary condition for pressure at the outlet (y = 1.6 m). Hence, the pressure at the inlet corresponds to the pressure drop across the turbine. From this figure, it can be observed that the pressure drop as the flow passes through the turbine rotor governs the main pressure distribution and the pressure fluctuations in the wake region. The reference turbine showed the largest pressure drop due to the high rotor solidity. The red and yellow lines in the figure indicate the pressure drop for turbines with serrations on the leading and trailing edges, respectively. Low rotor solidity results in a smaller pressure drop compared to the reference turbine. Furthermore, pressure fluctuations due to strong

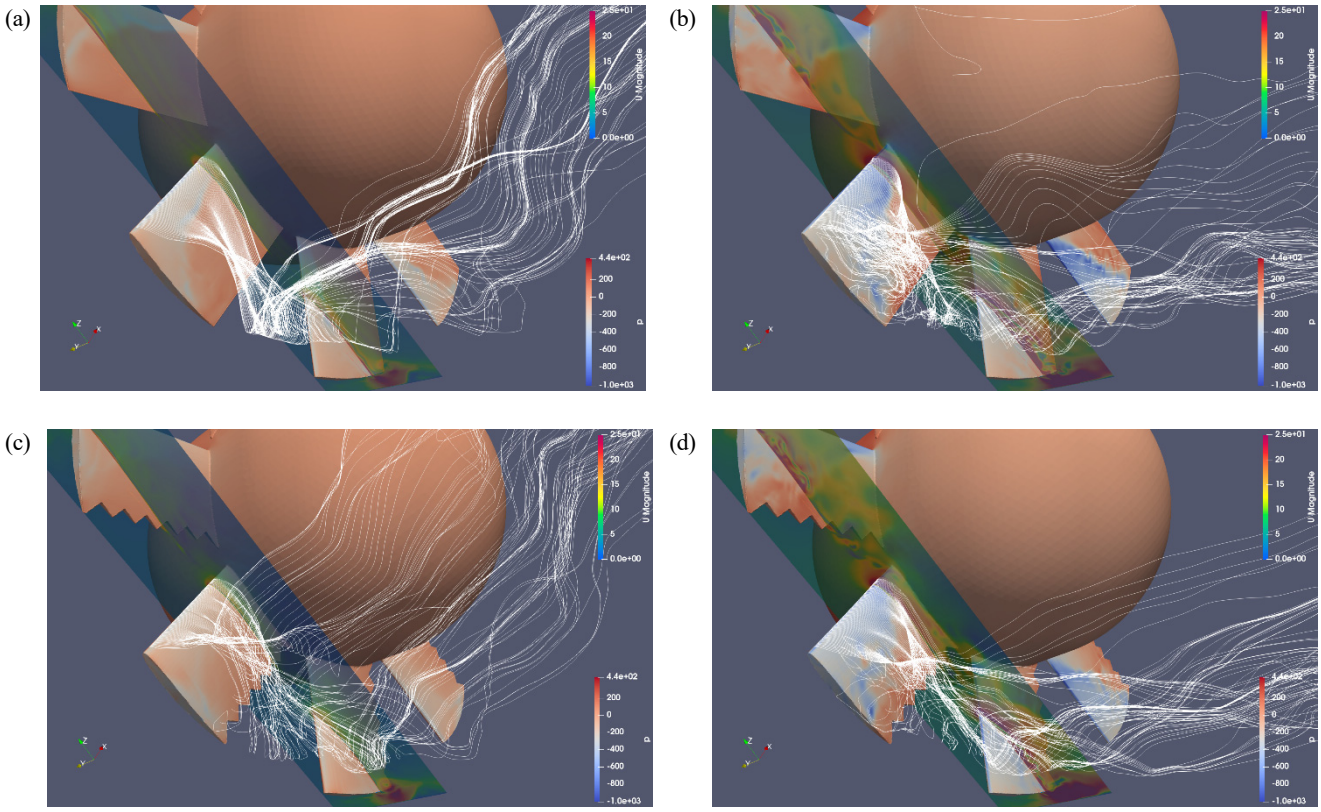

Fig. 11 Streamline behind the turbine blade and pressure on the turbine rotor for the reference turbine at t = 0.15 s (a) and t = 0.26 s (b) and for the T.E. serrated turbine at t = 0.15 s (c) and t = 0.26 s (d). The cropped plane shows the magnitude of the velocity around the blade.

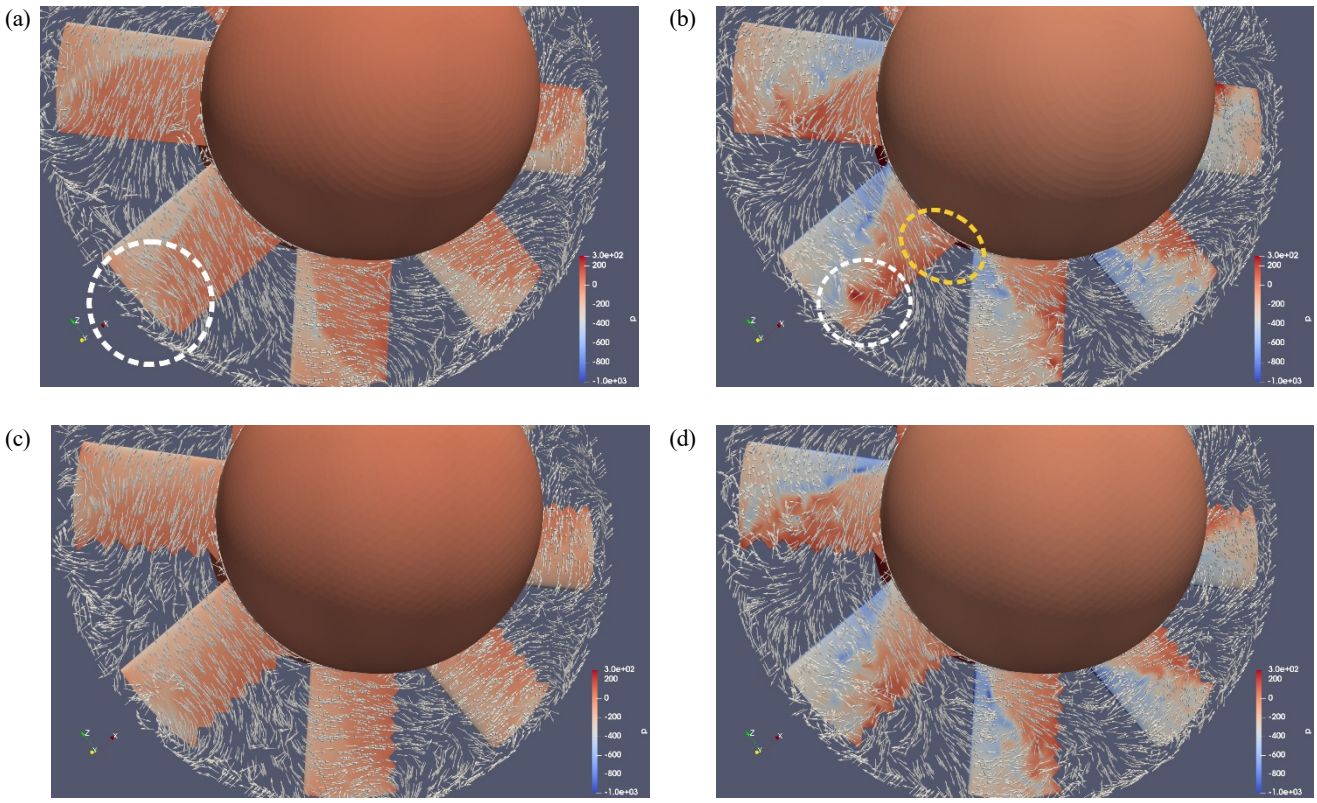

Fig. 12 Velocity vector behind the turbine. Reference turbine at t = 0.15 s (a) and t = 0.26 s (b), and T.E. serrated turbine at t = 0.15 s (c) and t = 0.26 s (d).

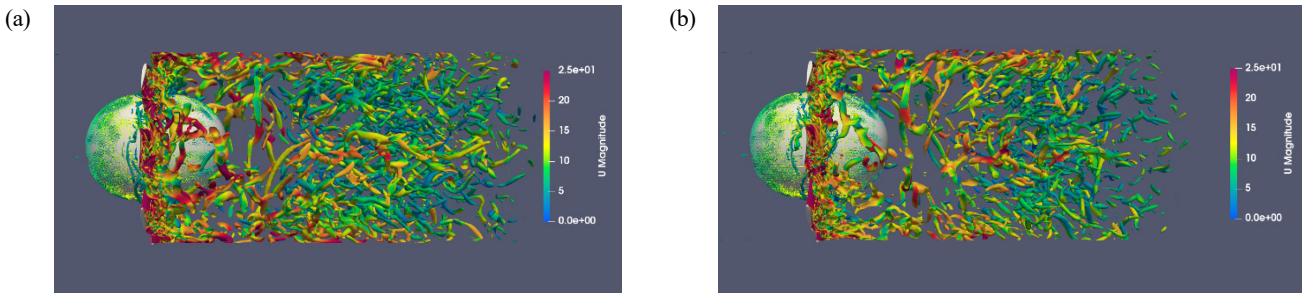

Fig. 13 Isosurface of the second invariant of velocity gradient tensor for reference turbine (a) and T. E. serrated turbine (b) at t = 0.3 s

turbulence in the wake are observed in the reference turbine, but these pressure fluctuations are suppressed in the serrated turbines. The suppression of pressure fluctuation is noticeable in the trailing edge serrated turbine. This suggests that the trailing edge serrations on the turbine blades suppress the pressure loss associated with large-scale separation of the flow.

Fig. 11 shows the flow patterns behind the turbine blade and pressure distribution on the turbine rotor for the reference turbine at t = 0.15 s (a) and t = 0.26 s (b) and for the T.E. serrated turbine at t = 0.15 s (c) and t = 0.26 s (d). In Figs. 11 (a) and (b), a clockwise swirling flow can be seen on the negative pressure side of the blade. Such a flow structure is formed closer to the rotor hub because the angle of attack increases as the inflow velocity increases. Furthermore, in Fig. 11(b), flow separation is also observed near the blade tip area, indicating that the blade is stalled in this case. In contrast, with serrated blades (Figs. 11 (c) and (d)), the position of the swirling flow formation moves towards the trailing edge of the blades. This suggests that flow separation near the leading edge of the blade is suppressed by the trailing edge serrations. This is consistent with the result that the trailing edge serrated turbine produces higher torque more consistently. The velocity distributions in the blade cross-sectional view also show that the wake formed by the forward blade interferes with the trailing blade leading edge region even at a high angle of attack. This means that the structure of the trailing edge serration may contribute to performance improvement of the Wells turbine.

The velocity vector behind the turbine blades is shown in Fig 12. This figure shows the velocity vector on a plane perpendicular to the rotating axis at a position 5 mm behind the turbine blades. Figs. 12 (a) and (b) show the reference turbine at t = 0.15 s and t = 0.26 s, and Figs. 12 (c) and (d) show the serrated turbine at t = 0.15 s and t = 0.26 s, respectively. In particular, in Figs. 12 (a) and (b), the presence of clockwise swirling flow on the back of the blades can be observed as

well as the streamline in Fig. 11 (white dashed circle). Furthermore, in Fig. 12 (b), the presence of reverse flow from the trailing edge side of the blade can be seen near the rotor hub (yellow dashed circle). In the case of the serrated turbine, the effect of stall is comparatively small because of the weak swirling flow and reverse flow behind the turbine. Such a strong clockwise swirling flow in the reference turbine has also been observed in experiments by Suzuki et al. (2008a), who stated that this reverse flow could induce a large-scale separation on the blade.

There are two possible reasons why trailing edge serrations in Wells turbines contribute to improved turbine performance. One is that the nature of the wake of the blade depends on the serration structure, and the other is that the addition of serrations reduces the turbine solidity, resulting in a lower pressure difference between the pressure and suction sides of the turbine. For the latter, however, this effect is limited, as torque increased by 50% despite a 5% decrease in solidity. As for the flow behavior of the wake region, Fig. 13 shows the structure of tip leakage vortices by isosurface of the second invariant of the velocity gradient tensor. These figures show typical spiral vortices generated from the blade tips. Vortices generated from the blade tips of the trailing edge serrated turbine are weaker than those of the reference turbine, and the vortex structure in the wake is also more sparse and weaker than in the reference turbine. This suggests that the addition of trailing edge serrations may contribute to the reduction of the tip leakage vortex and associated discrete frequency noise.

4. Conclusions

In this study, LES analysis was performed for a flow past an airfoil cascade and accelerated flow past a rotating Wells turbine. The results show that adding serrations to the trailing edge of the blade improves lift force and turbine torque over a wide range of operating conditions. The details are summarized as follows:

(1) Adding serrations to the trailing edge of the airfoil improved the stalling characteristics and lift-drag ratio.

(2) After stalling, there was no significant difference in the characteristics of the serrated and reference airfoils.

(3) The turbine axial torque increased with increasing inlet flow velocity for the trailing edge serrated turbine, but the reference turbine showed a decrease in performance due to stalling.

(4) The torque of the serrated turbine increased by up to 50% compared to the reference turbine.

(5) Flow field visualization revealed the structure of the separation and wake near the rotating blades. In addition, the serrated blades showed reduced flow separation.

(6) The results show that not only the interaction between serrated blades but also the serrations themselves have a significant effect on airfoil performance.

(7) The results suggest that trailing edge serrations may weaken the tip leakage vortex and contribute to the reduction of discrete frequency noise.

(8) The calculation results for the reference turbine agree qualitatively with existing experimental results.

Conflict of Interest

No potential conflict of interest relevant to this article is reported.

Funding

Funding from the Harada Foundation (https://harada-f.or.jp) is gratefully acknowledged.

References

Cao, H., & Zhang, M., Cai, C., & Zhang, Z. (2020). Flow topology and noise modeling of trailing edge serrations. *Applied Acoustics, 168*, 107423. https://doi.org/10.1016/j.apacoust.2020.107423

Cui, Y., & Hyun, B. (2016). Numerical study on Wells turbine with penetrating blade tip treatments for wave energy conversion. *International Journal of Naval Architecture and Ocean Engineering, 8*(5), 456-465. https://doi.org/10.1016/j.ijnaoe.2016.05.009

Hamakawa, H., Hani, K., Hayashi, H., & Kurihara, E. (2015). Aerodynamic noise radiated from Wells turbine at low flow rate condition. *Proceedings of the 13th Asian International Conference on Fluid Machinery*, 1-6.

Hussain, U., Malook, U. S., Shabir, B., & Ali, O. (2017). Effect of trailing edge serration on the lift and drag. *Proceedings of the 35th AIAA Applied Aerodynamics Conference*, 1-10.

Kotb, A. T. M., Nawar, M. A. A., Attai, Y. A., & Mohamed, M. H. (2023). (2003). Performance enhancement of a Wells turbine using CFD-oprimization algorithms coupling. *Energy, 282*, 128962. https://doi.org/10.1016/j.energy.2023.128962

Kumar, P. M,, Halder, P., Samad, A., & Rhee, S. H. (2018). Wave energy harvesting turbine: Effect of hub-to-tip profile modification. *International Journal of Fluid Machinery and Systems, 11*(1), 55-62. https://doi.org/10.5293/IJFMS.2018.11.1.055

Kurihara, E., Yasui, H., Isayama, Y., & Hamakawa, H. (2024). Numerical simulation of unsteady flow past a rotating wells turbine with modified blades. *Proceedings of the 7th Asian Offshore Wind, Wave and Tidal Energy Conference Series (AWTEC2024)*, p. 9.

Liu, X., Azarpeyvand, M., & Joseph, P. (2015). On the aerodynamic performance of serrated airfoils. *Proceeings of the 22nd International Congress on Sound and Vibration* (pp. 12-16).

Nicoud, F., & Ducros, F. (1999). Subgrid-scale stress modelling based on the square of the velocity gradient tensor. *Flow, Turbulence and Combustion, 62*, 183-200. https://doi.org/10.1023/A:1009995426001

Soltanmohamadi, R., & Lakzian, E. (2016). Improved design of Wells turbine for wave energy conversion using entropy generation.

Meccanica 51, 1713−1722. https://doi.org/10.1007/s11012-015-0330-x

Suzuki, M., & Arakawa, C. (2001). Numerical simulation of 3-D stall mechanism on wells turbine for wave-power generating system. *International Offshore and Polar Engineering, 11*(4), 315−320.

Suzuki, M., & Arakawa, C. (2008a). Guide vanes effect of Wells turbine for wave power generator. *International Offshore and Polar Engineering*, *10*(2), ISOPE-00-10-2-153.

Suzuki, M., & Arakawa, C. (2008b). Influence of blade profiles on flow around Wells turbine. *International Journal of Fluid Machinery and Systems 1*(1), 148−154. https://doi.org/10.5293/IJFMS.2008.1.1.148

Takao, M., Fukuma, S., Okuhara, S., Ashraful, A., & Kinoue, Y. (2019). A comparative study of bi-directional airflow turbines. *International Journal of Fluid Machinery and Systems*, *12*(3), 228−234. https://doi.org/10.5293/IJFMS.2019.12.3.228

Takao, M., Setoguchi, T., Kaneko, K., Raghunathan, S., & Inoue, M. (2002). Noise characteristics of turbines for wave power conversion. *Proceedings of the Institution of Mechanical Engineers, Part A: Journal of Power and Energy, 216*(3), 223−228. https://doi.org/10.1243/095765002320183540

Takao, M., Setoguchi, T., Kim, T. H., Kaneko, K., & Inoue, M. (2001). The performance of a Wells turbine with 3D guide vanes. *Internatinal Journal of Offshore Polar Engineering, 11*(1), 72−76.

Teruna, C., Avallone, F., Casalino, D., & Ragani, D. (2021). Numerical investigation of leading edge noise reduction on a rod-airfoil configuration using porous materials and serrations. *Journal of Sound and Vibration, 494,* 115880. https://doi.org/10.1016/j.jsv.2020.115880

Washio, Y., Osawa, H., Nagata, Y., Fujii, F., Furuyama, H., & Fujita, S. (2000). Offshore floating type wave power device “Mighty Whale”: Open sea teast. *Proceedings of the 10th Intlernational Offshore and Polar Engineering Conference*, ISOPE-I-00-054.

Author ORCIDs

Author name	ORCID
Kurihara, Eru	0009-0000-3795-4439
Yasui, Hiroki	0009-0002-9769-8793
Isayama, Yuito	0009-0003-0799-9216
Hamakawa, Hiromitsu	0009-0007-0800-7775